The effect of alkyl chain length in a series of novel N-alkyl-3-benzylimidazolium iodide salts

AUTHOR(S)

P Dean, J Golding, Jenny Pringle, Maria Forsyth, B Skelton, A White, D MacFarlane

PUBLICATION DATE

01-01-2009

HANDLE

10536/DRO/DU:30062931

The effect of alkyl chain length in a series of novel *N*-alkyl-3-benzylimidazolium iodide salts†

Pamela M. Dean,*[a] Jacob J. Golding,[a] Jennifer M. Pringle,[b] Maria Forsyth,[b] Brian W. Skelton,[c] Allan H. White[c] and Douglas R. MacFarlane[a]

Received 27th March 2009, Accepted 8th July 2009
First published as an Advance Article on the web 29th July 2009
DOI: 10.1039/b906142h

The crystal structures of a series of low-melting *N*-alkyl-2-methyl-3-benzylimidazolium iodide salts with a range of alkyl chain lengths, from $n = 1$ to 5 and including both *n*- and *s*-butyl chains, are reported for the first time. Thermal analysis shows that the methyl- and (*s*-)butyl substituted salts have significantly higher melting points than the rest of the series. Analysis of the crystal structures allows examination of the influence of the substituents on the different cation-anion and cation–cation interactions and thus the physical properties of the salts.

Introduction

The 1,3-dialkylimidazolium cation are widely employed in ionic liquid (IL) synthesis. These cations were first used in electrochemical studies as the dialkylimidazolium chloroaluminate ionic liquids which exhibited wider liquid and electrochemical ranges than those of the previously used alkylpyridinium based salts.[1] Furthermore, the imidazolium ILs display favourable physical properties such as high conductivities, solvation ability and wide range of Lewis acidity which, in addition to electrochemical applications,[2] allow for their utilisation in a variety of contexts such as cellulose dissolution,[3] metal-free catalysts,[4] lubricants[5] and for CO_2 separations,[6] to name just a few. In order to achieve novel applicative outcomes much research has been focused on designing novel ILs.[7,8] Their rational design however, requires a full understanding of the physicochemical properties of current ILs, and how these relate to intermolecular interactions. Several articles have been published detailing the structural analysis of imidazolium based ILs directed at assisting the understanding of the origin of their physical properties.[9–11] Variations in the length and/or degree of branching of the alkyl chain substituent, the addition of functional groups, and substitution at the C(2) position of the imidazolium ring may all influence their thermal behaviour.[12–14] In this work the crystal structures of a series of novel low-melting *N*-alkyl-2-methyl-3-benzylimidazolium iodide salts have been studied in order to assist a comparative understanding of the effects of the previously mentioned substituents within known ionic liquids. These analyses are beneficial since the 'anti crystal engineering' approach may be used: prior knowledge of intermolecular interactions and ionic dispositions found in 'traditional' ionic liquid compounds, combined with knowledge of those interactions which result in crystalline materials (as with the present array) can guide the avoidance of crystallization. Appropriate starting materials can then be selected which may result in ionic liquid formation.[15] Herein we report the crystal structures for: 1,2-dimethyl-3-benzylimidazolium iodide (**1**), 1-ethyl-2-methyl-3-benzylimidazolium iodide (**2**), 1-propyl-2-methyl-3-benzylimidazolium iodide (**3**), 1-(*n*-)butyl-2-methyl-3-benzylimidazolium iodide (**4**), 1-pentyl-2-methyl-3-benzylimidazolium iodide (**5**) and 1-(*s*-)butyl-2-methyl-3-benzylimidazolium iodide (**6**).

Results and discussion

Thermal analysis

The melting points for the series of *N*-alkyl-2-methyl-3-benzylimidazolium iodide salts are listed in Table 1. The three different substituents on the imidazolium group—the methyl, the benzyl and the various alkyl chains—are all expected to influence the melting point. It has previously been experimentally observed for a series of imidazolium salts with various counter-ions that

Table 1 Melting points of the *N*-alkyl-2-methyl-3-benzylimidazolium iodide salts

Compound	T_m (±1)/°C[a]
1,2-dimethyl-3-benzylimidazolium iodide (**1**)	154
1-ethyl-2-methyl-3-benzylimidazolium iodide (**2**)	86
1-propyl-2-methyl-3-benzylimidazolium iodide (**3**)	71
1-(*n*-)butyl-2-methyl-3-benzylimidazolium iodide (**4**)	61
1-pentyl-2-methyl-3-benzylimidazolium iodide (**5**)	61
1-(*s*-)butyl-2-methyl-3-benzylimidazolium iodide (**6**)	135

[a] DSC measurements carried out from −55 to 200 °C at a scan rate of 10 °C min^{-1}. Onset temperatures are reported in all cases.

[a]*School of Chemistry, Monash University, Clayton, Vic 3800, Australia. E-mail: pamela.dean@sci.monash.edu.au; Fax: +61(0)3 9905 4597*
[b]*Department of Materials Engineering and ARC Centre of Excellence in Electromaterials Science, Monash University, Clayton, Vic 3800, Australia*
[c]*Chemistry M313, School of Biomedical, Biomolecular and Chemical Sciences, University of Western Australia, Crawley, WA 6009, Australia*

† Electronic supplementary information (ESI) available: Analysis of the structures. CCDC reference numbers 711758, 711759, 720677–720680. For ESI and crystallographic data in CIF or other electronic format see DOI: 10.1039/b906142h

substitution at the C(2) position increases the melting point.[14] Although no direct comparison is possible, *N*-alkyl-2-methyl-3-benzylimidazolium iodide salts display higher melting points than those of *N*-methyl-3-alkylimidazolium iodide salts with analogous alkyl chain lengths.[16] The presence of the benzyl substituent was predicted to increase the melting point as a result of π–π interactions.

A well-known trend in typical 1-alkyl-3-methylimidazolium salts is the reduction of melting point with increasing alkyl chain length, up to $n = 8$. With $n > 8$ the compounds exhibit an increase in melting point, which is thought to be consequent on inter-chain hydrophobic packing with concomitant formation of bilayer-type structures.[12] Within the present benzyl-substituted series the reduction in melting point with increasing alkyl chain length is observed up to *n*-butyl, but with no further drop on progressing to the pentyl-substituted species. In addition, the 1-(*s*-)butyl-2-methyl-3-benzylimidazolium iodide salt displays a comparatively high melting point of 135 °C compared to that of 61 °C for 1-(*n*-) butyl-2-methyl-3-benzylimidazolium iodide. This is consistent with other reports in the literature which show that, with increased branching of the alkyl group, a comparative increase in melting point occurs, which is believed to be result from restricted rotational freedom.

Structural analysis

The general numbering scheme used for the *N*-alkyl-2-methyl-3-benzylimidazolium iodide salts for all analyses is outlined in Fig. 1 below. For ease of reference the salts will be referred to as 'alkyl-' from henceforth. More detailed crystallographic descriptions of the various salts are recorded in the ESI.

The methyl-, (*n*-)butyl- and pentyl-salts crystallise in orthorhombic lattices with eight, four and sixteen pairs of ions occupying the unit cell. The ethyl- and (*s*-)butyl- salts crystallise in monoclinic lattices, with eight and four pairs of ions within their unit cells. Lastly, propyl- crystallises in a triclinic lattice with two pairs of ions. All have one discrete ion pair, devoid of crystallographic symmetry, as the asymmetric unit of the structure, except ethyl- and pentyl- where there are two. The imidazolium rings of the cations for ethyl- were modelled as disordered over pairs of sites, occupancies 0.5 for cation 2, and 0.797(5) and complement for cation 1; for the pentyl- cation (2) two sites were identified for the γ- and δ- methylene groups. The crystal data for the structures are outlined in Table 2 below. One discrete ion pair for each new structure is shown as a thermal ellipsoid plot, along with the atom labelling scheme, in the ESI. As expected, the relative molar volume (V/Z) for the various salts increases as the length of the alkyl chain increases.

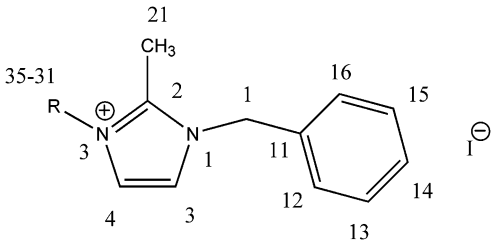

Fig. 1 Numbering scheme for the *N*-alkyl-2-methyl-3-benzylimidazolium iodide salts.

The dimensions of the C_3N_2 imidazolium ring skeletons (Table 3) do not vary non-trivially from each other or from those already reported.[10] The rings are planar with N(1)–C(2) and N(3)–C(2) being shorter than N(1)–C(5) and N(3)–C(4), indicative of charge delocalisation, at least over the N–C–N part of the ring (Table 3). The β-carbon atoms of the alkyl substituents for all of the iodide salts lie out of the planes of the imidazolium rings, as do the benzyl methylene groups, the planes of the phenyl rings lying *quasi*-parallel to C(2)–C(21) in all cases except that of molecule 1 of ethyl- where it is *quasi*- parallel to the N···N line (Table 3; torsion angles). In all cases, except molecule 2 of ethyl- and both molecules of pentyl-, the β-carbon atoms of the chains lie to the same side of the imidazolium planes as the benzyl groups. The alkyl chains for propyl- and cation (1) of pentyl- adopt the energetically preferred *trans*-oid configuration. In (*n*-)butyl- and cation (2) of pentyl- a *cis*-oid conformation is adopted, whilst (*s*-)butyl adopts the energetically favoured tetrahedral arrangement. The extended structures of methyl-, propyl- and (*n*-)butyl- show distinct layers of alternating anions and cations. By contrast, ethyl-, pentyl- and (*s*-)butyl- display clusters of anions and cations within zigzag-, brickwork-, and layered-type- arrangements (Fig. 2).

Although the precisions of the determinations of ethyl- and pentyl- are somewhat degraded by disorder, those of methyl-, *n*-, and *s*-butyl- are uncomplicated and nicely precise (Table 3), derivative of extensive data at 100 K, offering the possibility of comparing substituent effects between the three substituent types. The imidazole ring is 'symmetrically' substituted at the two nitrogen atoms by 'alkyl' substituents. Among the three complexes, without libration correction, the agreement between counterpart distances within the ring and to the immediate substituent carbon atoms is 0.00_7 Å or better, N(3)–C(31), the distance to the variable substituent excepted, where the range is 0.01_3 Å. Similarly, within the imidazole ring, agreement within the angles is excellent (better than $0.4°$) between 'symmetrically equivalent' counterparts. Around the ring periphery, however, considerable divergences are found; these may be understood to a considerable extent by consideration of intramolecular H···H contacts between the immediate CH_n substituent components rather than invoking 'lattice forces'. Thus, at N(1), C(1)–N(1)–C(2) is generally larger than C(1)–N(1)–C(5) in cognisance of the close contact between one of the CH_2 and one of the CH_3 hydrogen atoms, the location of the former being essentially constant by virtue of the reasonably constant out-of-plane C(2)–N(1)–C(1)–C(11) torsion angle (modulus); the dispositions of the CH_3 hydrogen atoms are more diverse, in consequence of interactions further afield. Similar observations and arguments obtain concerning the exocyclic angular differences about N(3), although they are less emphatic than those about N(1). It might be expected that the exocyclic angles at C(2) might be similar in view of the similar H···H interactions to either side, and this is generally true for the (*n*-)alkyl- derivatives. Unsurprisingly, however, the difference for (*s*-)butyl- is considerable, consequent on the more-or-less obligate in-plane disposition of the single C–H hydrogen atom. A converse asymmetry is observed in methyl- where the H···H distance is much longer, with concomitant diminution in N(3)–C(2)–C(21).

Table 2 Crystal data for the *N*-alkyl-2-methyl-3-benzylimidazolium iodide salts

	methyl- (**1**)	ethyl- (**2**)	propyl- (**3**)	(*n*-)butyl- (**4**)[a]	pentyl- (**5**)	(*s*-)butyl- (**6**)
Formula	$C_{12}H_{15}N_2I$	$C_{13}H_{17}N_2I$	$C_{14}H_{19}N_2I$	$C_{15}H_{21}N_2I$	$C_{16}H_{23}N_2I$	$C_{15}H_{21}N_2I$
M/Da	314.17	328.20	342.21	356.24	370.26	356.24
Crystal system	Orthorhombic	Monoclinic	Triclinic	Orthorhombic	Orthorhombic	Monoclinic
Space group	*Pbca* (#61)	$P2_1/c$ (#14)	$P\bar{1}$ (#2)	$P2_12_12_1$ (#19)	*Pbca* (#61)	$P2_1/c$ (#14)
a/Å	12.5337(1)	18.041(2)	8.232(2)	9.4229(1)	20.7565(3)	12.2127(2)
b/Å	11.6484(1)	11.085(1)	9.316(2)	11.8744(1)	14.0490(2)	11.3954(2)
c/Å	17.1447(2)	14.137(2)	10.209(3)	13.8521(1)	23.2945(4)	11.6217(2)
α/°			86.158(5)			
β/°		105.013(2)	86.638(5)			106.097(2)
γ/°			64.690(4)			
V/Å^3	2503	2731	704	1550	6793	1554
Z	8	8	2	4	16	4
(*V*/*Z*)/Å^3	313	341	352	388	425	389
D_c/g cm^{-3}	1.66_7	1.59_7	1.61_4	1.52_7	1.44_8	1.52_3
μ_{Mo}/mm^{-1}	2.5	2.3	2.3	2.1	1.88	2.05
Specimen/mm^3	0.51,0.26,0.17	0.63,0.50,0.12	0.43,0.40,0.35	0.49,0.27,0.16	0.35,0.31,0.23	0.49,0.35,0.21
$T_{min/max}$	0.66	0.77	0.90	0.67	0.74	0.62
$2\theta_{max}$/°	87	57	58	92	70	78
N_t	169801	22400	3613	58825	101051	34403
$N(R_{int})$	9534 (0.032)	7865 (0.027)	2190 (0.015)	13178 (0.034)	13863 (0.040)	8685 (0.028)
N_o	7484	6013	2107	11264	8921	7000
*R*1	0.019	0.033	0.024	0.023	0.057	0.021
*wR*2 (a(,b))	0.049 (0.026,0.22)	0.097 (0.049,1.01)	0.064 (0.038,0.49)	0.044 (0.019)	0.15 (0.068,10.9)	0.050 (0.025)
T/K	100	153	153	100	100	100

[a] *x*abs = −0.002(8).

Table 3 Selected cation core geometries for the *N*-alkyl-2-methyl-3-benzylimidazolium iodide salts

	methyl- (**1**)	ethyl- (**2**)[a] (mols. 1;2)	propyl- (**3**)	(*n*-)butyl- (**4**)	pentyl- (**5**)[a] (mols. 1;2)	(*s*-)butyl- (**6**)
Distances/Å						
C(1)–C(11)	1.5066(10)	1.510(4)/–; 1.508(5)/-	1.507(4)	1.509(1)	1.504(5); 1.523(6)	1.515(1)
N(1)–C(2)	1.3432(9)	1.347(5)/1.349(13); 1.346(7)/1.305(9)	1.321(5)	1.344(1)	1.312(5); 1.327(5)	1.343(1)
N(1)–C(5)	1.3838(9)	1.387(5)/1.395(14); 1.378(13)/1.393(9)	1.378(3)	1.382(1)	1.417(6); 1.404(5)	1.384(1)
N(1)–C(1)	1.4761(9)	1.458(4)/1.432(11); 1.570(7)/1.394(7)	1.479(4)	1.475(1)	1.466(5); 1.488(5)	1.471(1)
C(2)–N(3)	1.3409(9)	1.335(4)/1.317(14); 1.340(7)/1.335(10)	1.339(4)	1.337(1)	1.319(5); 1.338(5)	1.340(1)
C(2)–C(21)	1.4805(10)	1.465(5)/1.456(14); 1.480(9)/1.483(14)	1.481(4)	1.482(1)	1.476(6); 1.481(6)	1.481(1)
N(3)–C(4)	1.3818(10)	1.388(5)/1.397(15); 1.376(7)/1.406(10)	1.374(4)	1.380(1)	1.420(6); 1.402(5)	1.387(1)
N(3)–C(31)	1.4675(10)	1.464(4)/1.505(11); 1.380(6)/1.532(8)	1.471(4)	1.474(1)	1.452(5); 1.469(5)	1.481(1)
C(4)–C(5)	1.3540(11)	1.348(5)/1.353(16); 1.345(12)/1.324(10)	1.348(4)	1.360(1)	1.294(7); 1.317(6)	1.356(1)
H(21X)···H(31Y)(X,Y)	2.56(A,C)	2.21(A,B)/2.02(C′,F); 2.44(C,D)/2.75(C,D)	2.22(B,B)	2.25(A,B)	2.44(B,D); 2.19(A,A)	2.17(A,-)
H(21X)···H(1Y)(X,Y)	2.09(B,A)	2.14(A,B)/2.39(B,D); 2.12(B,B)/1.94(A,D)	2.21(C,A)	2.19(B,A)	2.23(B,A); 2.31(B,A)	2.20(B,A)
Angles/°						
N(1)–C(1)–C(11)	111.98(6)	113.0(3)/115.7(4); 110.1(3)/112.2(3)	111.9(2)	111.93(7)	109.4(3); 111.9(3)	111.29(8)
C(1)–N(1)–C(2)	127.12(6)	127.5(3)/126.6(10); 125.2(5)/123.0(7)	127.6(2)	126.95(8)	128.8(4); 127.3(3)	125.74(9)
C(1)–N(1)–C(5)	123.64(6)	123.2(3)/123.5(10); 126.0(7)/128.5(6)	122.9(3)	123.70(8)	124.1(4); 124.2(3)	124.82(8)
C(2)–N(1)–C(5)	109.14(6)	109.3(3)/109.9(10); 108.6(7)/108.2(7)	109.4(2)	109.35(8)	106.8(4); 108.4(3)	109.19(8)
N(1)–C(2)–C(21)	128.18(6)	126.1(4)/126.1(13); 126.4(6)/126.6(11)	127.1(3)	126.73(9)	126.0(4); 125.5(4)	125.39(9)
N(3)–C(2)–C(21)	124.36(6)	126.6(4)/127.0(14); 126.3(6)/124.1(9)	124.9(3)	125.90(9)	123.4(4); 126.0(4)	126.99(9)
N(1)–C(2)–N(3)	107.46(6)	107.3(3)/106.9(10); 107.3(5)/109.3(7)	108.0(3)	107.36(8)	110.5(4); 108.5(3)	107.62(8)
C(2)–N(3)–C(31)	125.01(6)	126.4(3)/126.910); 127.3(5)/137.4(7)	126.4(3)	126.16(9)	131.4(4); 129.4(4)	126.59(8)
C(4)–N(3)–C(31)	125.56(6)	124.0(3)/122.6(10); 123.1(5)/114.3(6)	124.9(2)	124.24(8)	121.6(4); 122.6(3)	124.12(8)
C(2)–N(3)–C(4)	109.35(6)	109.4(3)/110.3(11); 109.6(5)/107.9(7)	108.7(3)	109.60(8)	107.0(4); 108.0(3)	109.23(8)
N(3)–C(4)–C(5)	107.00(6)	107.1(3)/106.8(13); 106.8(7)/106.2(8)	107.3(2)	106.87(9)	107.4(4); 107.7(4)	106.89(9)
C(4)–C(5)–N(1)	107.06(6)	106.9(4)/106.0(12); 107.8(9)/108.3(7)	106.6(3)	106.82(9)	108.3(4); 107.4(4)	107.07(8)
Torsion angles/°						
C(2)–N(3)–C(31)–C(32)	—	−88.2(4)/113.9(13); 86.5(7)/−114.4(1)	−80.0(4)	−82.6(1)	86.7(6);117.3(5)	127.1(1)[b]
C(2)–N(1)–C(1)–C(11)	118.68(7)	101.3(4)/−97.7(13); 91.3(6)/−88.8(8)	109.9(4)	94.7(1)	96.2(5);91.6(5)	79.2(1)
N(1)–C(1)–C(11)–C(ortho)	−81.60(8)	−15.1(4)/22.0(7); −86.9(4)/−50.1(5)	−79.8(3)	80.6(1)	−85.7(4);86.8(4)	70.0(1)
C(2)–N(3)–C(31) –H(31A)	–66	150/−32; −36/138	158	156	−34; –3	-[b]
–H(31B)	174	33/−139; −151/28	42	38	−152; −122	—
–H(31C)	54					
N(1)–C(2)–C(21) –H(2A)	120	150/63; 131/–13	-83	147	−89; −69	147
–H(2B)	0	30/−57; 11/–133	157	27	151;171	27
–H(2C)	–120	–90/−177; −109/107	37	–93	31;51	−93

[a] Two independent molecules; in **2**, each molecule has two independent components. [b] C(2)–N(3)–C(31)–C(33),H are −108.4(1),9.3°.

The type and extent of interspecies interactions within a salt have a direct influence on its physical properties, such as the melting point. These interactions, which may encompass long-range coulombic and short-range weak attractive forces, are dependent on the component geometries and charge distributions. Organic ions tend to be bulky and have an unsymmetrical

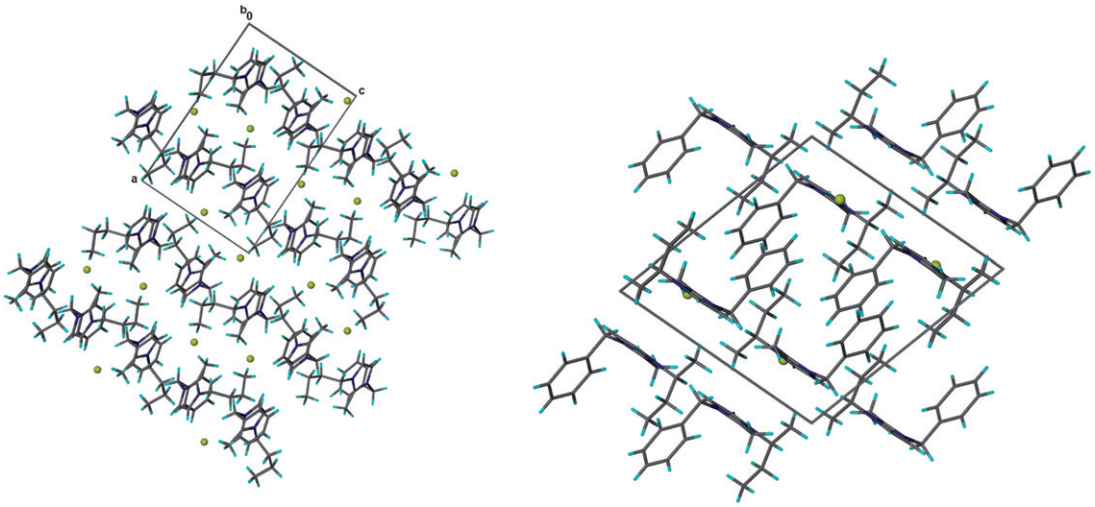

Fig. 2 Packing diagrams as viewed down the *b*-axes for (a) 1-(*n*-)butyl-2-methyl-3-benzylimidazolium iodide (**4**) and (b) 1-(*s*-)butyl-2-methyl-3-benzylimidazolium iodide (**6**).

charge distribution which should increase the likelihood of directional short-range contacts and slightly decrease the strength of the coulombic forces.[17,18] However, lattice energy calculations, beyond the scope of this structural analysis, are required to fully understand the long-range coulombic effect within each salt. Analysis of the ion-pair suggests that the orientation of the anion *vis-a-vis* the cation should be of importance as the interaction energy is to some extent influenced by the distance between the anion and the imidazolium ring.[17] Table 4 displays the shortest cation-anion separations in each compound, as represented by the nominal centres of positive (N atom, either N(1) or N(3)) and negative (X atom) charge. As expected, most of the closest contacts occur towards the alkylated N(3) atom at the face of least steric hindrance. In (*s*-)butyl-, the closest contact is found where the anion is located directly above the plane of the ring towards the C(2) atom. Methyl- also displays the anion very nearly directly over the plane of the ring; all others reflect a side-on approach towards the C(4)/C(5) side of the ring. Interaction energies have previously been calculated using quantum chemical methods for various orientations and distances for a series of *N*-alkylimidazolium salts[17,18] and it was found that the calculated interaction energy is inversely proportional to the distance between the ions and that the

Table 4 Comparison of the closest cation–anion I···N distances (Å) of the *N*-alkyl-2-methyl-3-benzylimidazolium iodide salts.[a]

Compound	I···N(1)	I···N(3)
methyl- (**1**)	—	4.4514(7)^{i}
ethyl- (**2**)	4.429(3)	4.24(1)^{ii}
propyl- (**3**)	4.354(3)^{iii}	4.389(3)
(*n*-)butyl- (**4**)	4.4174(8)^{iv}	4.3796(8)^{v}
pentyl- (**5**)	4.376(3)^{vi}	4.461(3)^{vii}
(*s*-)butyl (**6**)	4.0064(9)^{viii}	3.8604(8)^{viii}

[a] Symmetry transformations of I: (i) $1-x, y-\frac{1}{2}, \frac{3}{2}-z$; (ii) $2-x, 1-y, 1-z$; (iii) $\bar{x}, 2-y, 1-z$; (iv) $x+\frac{1}{2}, \frac{1}{2}-y, 1-z$; (v) $\frac{1}{2}-x, 1-y, z-\frac{1}{2}$; (vi) $1-x, y+\frac{1}{2}, \frac{1}{2}-z$; (vii) $x-\frac{1}{2}, \frac{1}{2}-y, 1-z$; (viii) $1-x, 1-y, 1-z$.

Table 5 I···H–C distances (<3.3) (Å) found in the *N*-alkyl-2-methyl-3-benzylimidazolium iodide salts.[b]

	C(1)	C(4)	C(5)	C(21)	C(31–35)	C(11–16)
methyl- (**1**)	3.15	3.15^{i}	3.03^{ii}	3.20^{iii}	3.05^{iv}	3.30^{v}
ethyl- (**2**)	3.08^{i},3.20 (3.16^{ii})[a]	–(3.06^{iii})	3.04 (2.98^{ii})	–(–)	–(3.19)	–(3.25^{iv})
(I(1))						
(I(2))	3.09 (–)	–(2.98^{v}, 2.90^{vi})	3.07 (–)	3.18 (3.10^{iv},3.27^{vi})	3.18 (3.02^{vi},3.19^{v},3.17^{ii},3.20^{iv})	3.21 (3.25^{iv})
propyl- (**3**)	3.13^{i},3.17^{ii}	3.09	– (–)	3.01^{ii}	3.14,3.14^{iii}	3.28^{iv},3.23^{v}
(*n*-)butyl- (**4**)	3.17^{i}	3.07^{ii}	3.13^{i}	3.06,3.16^{iii}	3.12^{iii},3.16^{ii}	—
pentyl- (**5**)	2.98(3.16^{i}, 2.99^{ii})	– (–)	–(3.20^{i})	3.15(3.21^{ii})	3.12^{iii} (–)	3.13^{iv} (3.30^{i})
(I(1))						
(I(2))	– (–)	–(2.80^{iv})	–(2.98^{vi})	– (–)	3.18^{vii}, 3.24^{viii} (–)	– (–)
(*s*-)butyl- (**6**)	3.18^{i}	3.01^{ii}	3.22^{i}	– (–)	3.16^{iii},3.29^{ii}	3.29^{iv}

[a] The values in parentheses correspond to the other cationic component of the asymmetric unit. [b] Symmetry transformations of H: (**1**) (i) $\frac{1}{2}-x, \frac{1}{2}+y, z$; (ii) $\frac{1}{2}+x, \frac{1}{2}-y, 1-z$; (iii) $\frac{1}{2}+x, y, \frac{3}{2}-z$; (iv) $1-x, \frac{1}{2}+y, \frac{3}{2}-z$; (v) $x, \frac{1}{2}-y, \frac{1}{2}+z$. (**2**) (i) $x, \frac{1}{2}-y, z-\frac{1}{2}$; (ii) $x, y-1, z$; (iii) $1-x, y-\frac{1}{2}, \frac{1}{2}-z$; (iv) $x, \frac{3}{2}-y, z-\frac{1}{2}$; (v) $2-x, \frac{1}{2}+y, \frac{1}{2}-z$; (vi) $2-x, 1-y, 1-z$ (**3**) (i) $\bar{x}, 2-y, 1-z$; (ii) $x, y, z-1$; (iii) $\bar{x}, 1-y, 1-z$; (iv) $1-\bar{x}, 1-y, 1-z$; (v) $1-x, 2-y, 1-z$. (**4**) (i) $x-\frac{1}{2}, \frac{1}{2}-y, 1-z$; (ii) $\frac{1}{2}-x, 1-y, \frac{1}{2}+z$; (iii) $1-x, y-\frac{1}{2}, \frac{3}{2}-z$. (**5**) (i) $\frac{1}{2}-x, \frac{1}{2}+y, z-1$; (ii) $x, y, z-1$; (iii) $\frac{1}{2}-x, \frac{1}{2}+y, z$; (iv) $1/2+x, 3/2-y, \bar{z}$; (v) $1+x, y, z$; (vi) $1-x, y-\frac{1}{2}, \frac{1}{2}-z$; (vii) $\frac{1}{2}+x, \frac{1}{2}-y, 1-z$; (viii) $\frac{3}{2}-x, 1-y, z-\frac{1}{2}$. (**6**) (i) $x, y, z-1$; (ii) $x, \frac{1}{2}-y, z-\frac{1}{2}$; (iii) $1-x, 1-y, 1-z$; (iv) $x, \frac{3}{2}-y, z-\frac{1}{2}$.

disposition with the anion located above the C(2) atom of the ring was more energetically preferred to that of the near in-plane position towards C(4)/C(5). Thus (*s*-)butyl- and methyl- display the energetically preferred ion pair conformation, with (*s*-)butyl- displaying the closest contact. This is consistent with the higher melting points of these two salts.

In addition to short anion–cation interactions, an increase in short-range weakly attractive forces such as hydrogen bonding or π–π stacking between the ions could theoretically increase the melting point. These interactions are highly directional and are known to be energetically weaker than isotropic charge–charge interactions.[17] However, the additive effect of these forces should contribute to the total energy of the salt. This series of *N*-alkyl-2-methyl-3-benzylimidazolium iodide salts provides a useful model to study the effects of π–π stacking as a result of the presence of a benzyl substituent. In addition the result of C(2)-methylation may be analysed.

No classical hydrogen bonding is observed, owing to a lack of directionality (no D–H···A > 100° observed), so that, for the purpose of assessing close-contact interactions, distances are reported which are limited to those within the sum of the van der Waals radii (*e.g.* H···I ~3.0_4-3.2_4 Å). For π–π stacking the centroid to centroid distance is less than 3.8 Å with an interplanar angle less than 60°.[19] The ions in the salts of methyl-, ethyl-, propyl- and pentyl- are interconnected by a 3D network of weak C–H···I contacts, those in (*s*-)butyl, and (*n*-)butyl- being connected in a 2D array, as outlined in Table 4. For the ethyl- and pentyl-substituted salts, analyses of C–H···X, C–H···π and π···π interactions are complicated by cation disorder.

A comparison of crystalline *N*-methyl-3-alkylimidazolium halide salts[10] and the *N*-alkyl-2-methyl-3-benzylimidazolium iodide salts shows that, with methylation of the imidazolium ring at the 2-position, an equal or greater number of non-classical hydrogen bonds are still observed. In addition, very short C–H···I contacts comparable to the acidic C(2)–H distance of [C_2mim]I are also observed in the methyl-substituted salts, particularly at the C(4) and C(5) positions (Table 5). A previous theoretical study on a series of *N*-methyl-3-alkylimidazolium salts with various counter-ions indicate that orientation dependent dipole–dipole interactions, *i.e.* linear C–H···X hydrogen bonds, are not experimentally observed, thus suggesting that the influence of hydrogen bonding at the C(2) position is not particularly significant, and that charge–charge interactions predominate.[17,20] Interestingly, [C_2mim]I also does not display a linear C–H···I hydrogen bond; the angle is 144(3)°, which is not regarded as a classical hydrogen bond.[10] Again, within this series, no classical hydrogen bonding is observed between C(4) and C(5) of the cation and the anion, suggesting coulombic interactions to be dominant.

No π–π stacking is observed between the imidazolium aromatic rings in the salts, further suggesting that ionic forces (in this case repulsion) dominate the interspecies interactions of these salts. π–π stacking is observed between the benzyl aromatic rings for propyl- and between the benzyl and imidazolium rings for methyl- and ethyl- (Table 6); in all other structures either the interplanar distance is too great or the rings are too canted with respect to each other to allow for these interactions. However C–H···π interactions between the benzyl group and either an alkyl chain or another perpendicular benzyl group do arise (see Table 7). Due to the steric hindrance of the (*s*-)butyl group, this salt does not exhibit any π···π or C–H···π interactions. methyl-, which displays the highest melting point, exhibits both π···π and C–H···π interactions, reflecting the contribution of the benzyl group to the increased melting point.

Hirshfeld surface generation and fingerprint plot analysis

The Hirshfeld Surface Analysis has been found to be useful in understanding the intricacies of interactions occurring in crystallised ionic liquids.[21] A Hirshfeld Surface Analysis has been performed for a number of the salts, producing a Fingerprint plot for each cation of the structures, Fig. 3; analysis was not conducted on ethyl- and pentyl- because of disorder.‡

Decomposed Fingerprint plots are presented in the ESI. As part of this decomposition analysis, the fraction of the Hirshfeld surface representing a given interaction was calculated (Table 8).

Of the *N*-alkyl-2-methyl-3-benzylimidazolium iodide salts, methyl- displays the greatest contribution of the C–H···I interaction compared to the other types of interactions; this also has closer contacts than the other interactions (as indicated by the diagonal lines on the plots in the ESI) and thus a higher contributing attractive energy. This is consistent with the higher melting point. In the region greater than $d_i + d_e = 2.2$ Å all of the plots become quite scattered, indicating a number of points on the surface having separations distinctly greater than the sum of the van der Waals radii. All salts except (*n*-)butyl-, indicate the closest C–H···I interaction at d_e, d_i ~1.9, 1.0 Å; (*n*-)butyl-, with the lowest melting point, shows a longer distance at d_e, d_i ~1.95, 1.09 Å. The largest contribution of close contact C–H···H interactions (see diagonal lines of the plots within the ESI) and π–π interactions occurs once again for methyl-, which is consistent with the highest melting point for this salt. Interestingly, for the overall total contribution of C–H···H interactions

‡ The program CrystalExplorer 2.0 was used to generate all surfaces and fingerprint plots. The Hirshfeld Surface is defined so that for each point on the surface '1/2 of the electron density is due to the spherically averaged non-interacting atoms comprising the molecule, and the other half is due to those comprising the rest of the crystal'.[23] So, the surface contains 'a region of space surrounding a particular molecule in a crystal where the electron distribution of that molecule exceeds that due to any other molecule'.[23] Close contacts can then be shown on this surface by calculating a normalised contact distance, d_{norm}, which compares the distance between two atoms across the surface to the combined van der Waal radii of the atoms.[24] The Hirshfeld surface can then be thought of as an 'interaction surface' that highlights and identifies important interactions in the crystal. Hirshfeld Surfaces and their associated Fingerprint Plots were generated using the program CrystalExplorer.[25] The Fingerprint Plot plots the distance (d_i) from the nearest atom inside the surface against the distance (d_e) to the nearest atom external to the surface; the Fingerprint Plots for all of the selected salts are presented in the Supplementary Information. The Fingerprint Plot provides information on the fraction of the Hirshfeld Surface area due to any particular contact and how extensive that fraction is in distance. The colour coding in the Fingerprint Plot represents the frequency of occurrence of any given (d_i,d_e) pair with white = no occurrence, blue = some occurrence, and green then red indicating more frequent occurrence. For further detailed analysis, Crystal Explorer also allows the isolation of any given interaction (*e.g.* C–H···I) and then the generation of a 'decomposed' fingerprint plot, where only the relevant interactions are coloured, and the associated Hirshfeld surface coloured for that interaction alone.[23] Decomposed Fingerprint plots for the other interactions are presented in the Supplementary Information.

Table 6 Closest π···π ring interaction distances (<4 Å) (Å)[b]

	Cg(1)···Cg(1)[a]	Cg(2)···Cg(2)	Cg(1)···Cg(2)
methyl- (**1**)	—	3.71[i]	3.45[ii]
ethyl- (**2**)	—	—	(3.73/3.77)[iii] (3.80/3.87)[iv]
propyl- (**3**)	—	3.72[v]	

[a] Cg(1) is the centroid of the imidazolium ring and Cg(2) of the benzyl ring. Values in parentheses are to molecule 2 of the asymmetric unit. [b] Symmetry transformations (second centroid): (i) $1-x, \bar{y}, 1-z$; (ii) $x-\frac{1}{2}, \frac{1}{2}-y, 1-z$; (iii) $x, y-1, z$; (iv) $x, {}^{3}/_{2}-y, z-\frac{1}{2}$; (v) $1-x, 2-y, 2-z$.

Table 7 Close C–H···π ring interaction distances (<3 Å) (Å).[b]

	X_{donor}–H	H···Cg(1)[a]	H···Cg(2)
methyl- (**1**)	C(14)–H(14)	2.76[i]	—
ethyl- (**2**)	C(113)–H(113)	—	2.78
propyl- (**3**)	C(14)–H(14)	2.90[ii]	—
	C(32)–H(32B)	2.96[iii]	—
(*n*-)butyl- (**4**)	C(32)–H(32B)	—	2.71[iv]
pentyl- (**5**)	C(135)–H(13I)	—	(2.70[v])
	C(135)–H(13J)	(2.71)[v]	
	C(135)–H(13K)	2.61[vi]	

[a] Cg(1) is the centroid of the imidazolium ring and Cg(2) of the benzyl ring. The values in parentheses correspond to the second cationic component of the asymmetric unit. [b] Symmetry transformations of H: (i) $1-x, \bar{y}, 1-z$; (ii) $x-1, y, z$; (iii) $1-x, 1-y, 1-z$; (iv) $\frac{1}{2}+x, \frac{1}{2}-y, 1-z$; (v) $x, \frac{1}{2}-y, \frac{1}{2}+z$; (vi) $\frac{1}{2}-x, y-\frac{1}{2}, z$.

(*s*-)butyl- displays a significantly higher percentage of 73.9 to that of 66.8 for (*n*-)butyl-, indicating that branching increases the likelihood of short and long contacts, which would overall contribute to the attractive energy thus increasing the melting point relative to the *n*-butyl species. No definitive trends are seen for the relative percentage contributions for C–H···π contacts across the series, suggesting that the C–H···I and π–π interactions have a greater energetic contribution *cf.* C–H···π contacts. By general comparison of the shapes of the plots it is apparent that methyl- and propyl- display the most compressed plots within d_e and d_i, suggesting more compact packing of these salts. (*n*-)butyl-, with the lowest melting point, displays a greater spread in d_e which suggests non-optimum packing with a larger distance between neighbouring cations, which is consistent with their long alkyl chains. Lastly, (*s*-)butyl- displays the greatest spread in d_i, reflecting the size and asymmetry of this cation. Noticeable within all the salts is a larger number of particularly long contacts > 4 Å; such long contacts are evidence of 'voids' in the structure and non-optimum packing, thus resulting, overall, in generally low melting salts.

The mean value of d_{norm}, over the whole of the Hirshfeld Surface, has been calculated for each Surface (Table 9). This average can be thought of as a measure of packing efficiency and therefore also of relative free volume in the structure. This provides a useful connection between the structure and the melting point since this is believed in some models[22] to be dependent on free volume. If this quantity is small, the packing of the cation is more compact, thus leading one to expect that the melting point of the salt should be uniformly higher. (*n*-)butyl- and (*s*-)butyl- display the largest d_{norm}

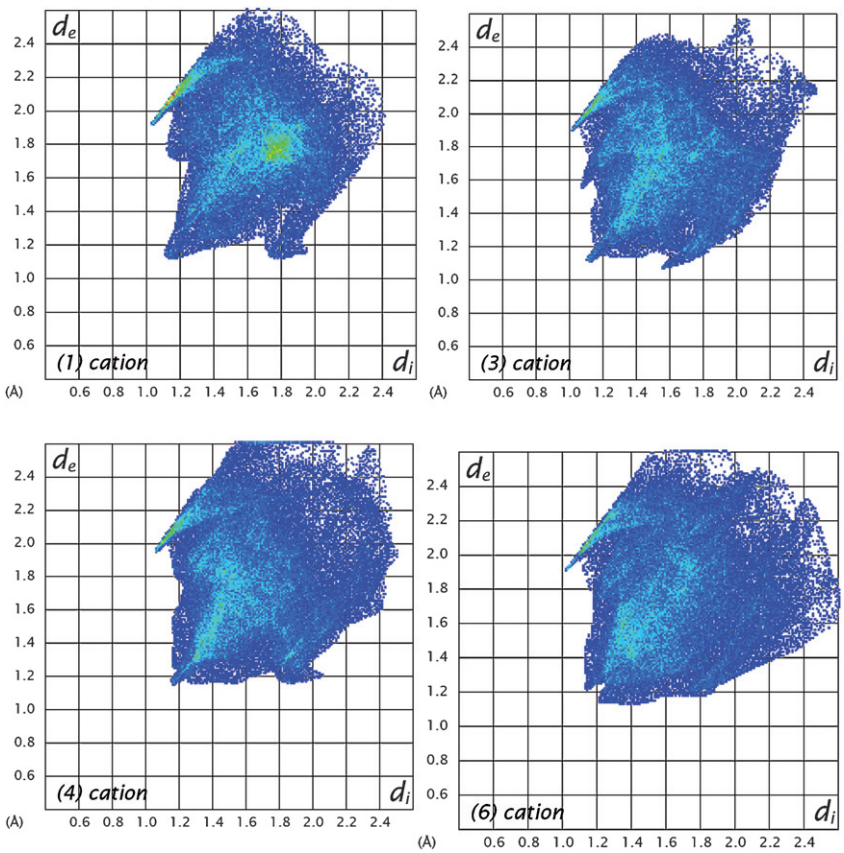

Fig. 3 Full Fingerprint plots for the cations of (**1**) methyl-, (**3**) propyl-, (**4**) (*n*-)butyl and (**6**) (*s*-)butyl.

Table 8 Relative percentage contributions of selected cation–anion and cation–cation contacts for the *N*-alkyl-2-methyl-3-benzylimidazolium iodide salts (relative to the whole of the Hirshfeld surface area[a])

%	methyl- (**1**)	propyl- (**3**)	(*n*-)butyl- (**4**)	(*s*-)butyl- (**6**)
C–H···I	9.9	8.2	9.6	8.6
C–H···H	65.7	66.5	66.8	73.9
C···H/H···C[b]	13.1	18.9	20.7	15.6
N···H/H···N[b]	2.6	3.8	2.0	0.3
C···C[b]	6.5	2.5	0.1	0.0

[a] See ESI for full details of Fingerprint Plots. [b] C and N indicate the π contributions of the aromatics. The reciprocal contact relative contributions are shown.

Table 9 Comparison of the mean d_{norm} of the *N*-alkyl-2-methyl-3-benzylimidazolium iodide and [C_2mim]I Hirshfeld Surfaces

Compound	d_{norm}
methyl- (**1**)	0.4149
propyl- (**3**)	0.3767
(*n*-)butyl- (**4**)	0.4598
(*s*-)butyl- (**6**)]	0.4793

values indicating a less packed structure. A large d_{norm} value is expected for (*s*-)butyl- due to the sterically demanding branched alkyl chain, but, interestingly, (*n*-)butyl-, which displays the lowest melting point in this series, also displays a large d_{norm} value, thus confirming that the less compact packing of this salt is associated with a lower melting point. However, the similarity of these results confirms that the predominant interaction in all cases is the charge–charge interaction.

Conclusion

A series of novel *N*-alkyl-2-methyl-3-benzylimidazolium iodide salts, with a range of alkyl chain lengths, have been prepared and analysed with respect to the influence of the various substituents on the crystal structure. Overall, the dominant interaction in all of the structures is isotropic charge–charge interaction, which is consistent with the previously-reported imidazolium salts. The presence of the benzyl group results in significant π–π stacking only in the methyl-substituted salt, and this salt also exhibits the strongest contribution of the cation-anion (C–H···I) interaction, which is consistent with its high melting point. The salts with the longer alkyl chains form less closely packed structures, with no direct π–π interactions or classical hydrogen bonds. Hirshfeld surface analysis indicates that the use of a branched alkyl chain increases the overall total contribution of C–H···H interactions compared to the straight chain analogues, which will contribute to the higher melting point. Such analysis is invaluable in building up an understanding of all of the interactions occurring in crystallised low melting organic salts and thus ultimately allowing the target-specific design of new materials.

Experimental

N-Alkylation of 1-benzyl-2-methylimidazole—general procedure

1-Benzyl-2-methylimidazole (95%, Aldrich) was dissolved in a minimum of dry acetonitrile and an excess (approx. 2.5 equiv.) of the appropriate alkyl halide (used as received (Aldrich/BDH/Fluka)) added. The solution was stirred vigorously for between 4–6 h. Dry diethyl ether was added to the solution until no more solid precipitated (some alkyl substituents may lead to a separation of two liquid phases). The 1-alkyl-2-methyl-3-benzylimidazolium iodide was then isolated by filtration and washed three times with 20 ml of dry diethyl ether.

1,2-Dimethyl-3-benzylimidazolium iodide (1). 1-Benzyl-2-methylimidazole (6.25g, 36.5 mmol) and methyl iodide (15g, 105 mmol) were combined to yield 1,2-dimethyl-3-benzylimidazolium iodide (10.02g, 88%); ν_{max}(KBr)/cm^{-1} 3163, 3116, 3070, 3037, 2990, 2935, 1642, 1583, 1533, 1498, 1459, 1425, 1391, 1378, 1353, 1324, 1250, 1238, 1210, 1154, 1105, 1089, 1047, 1032, 966, 943, 910, 875, 830, 774, 722, 692 and 663. δ_H (200 MHz; $CDCl_3$; Me_4Si) 2.80 (3H, s, C(21)H), 3.95 (3H, s, C(31)H), 5.50 (2H, s, C(1)H), 7.37 (5H, br.s, C(12–16)H), 7.48 (1H, d, C(4)H), 7.61 (1H, d, C(5)H); δ_C (50 MHz; $CDCl_3$; Me_4Si) 12.32 (C21), 36.77 (C31), 52.74 (C1), 121.64 (C4), 122.89 (C5), 128.48 (C13,15), 129.32 (C14), 129.53 (C12,16), 132.62 (C11), 144.16 (C2). *m*/*z* (ES$^+$) 187.1, 188.2; *m*/*z* (ES$^-$) 126.9; mp onset 153.6 °C, peak 155.5 °C, *J*/g = 84.2.

1-Ethyl-2-methyl-3-benzylimidazolium iodide (2). 1-Benzyl-2-methylimidazole (10.6g, 61.9 mmol) and ethyl iodide (20g, 128 mmol) were combined to yield 1-ethyl-2-methyl-3-benzylimidazolium iodide (15.2g, 75%); ν_{max}(KBr)/cm^{-1} 3169, 3113, 3071, 3030, 2974, 1604, 1584, 1527, 1496, 1450, 1386, 1354, 1267, 1208, 1161, 1124, 1090, 1032, 973, 954, 852, 806, 762, 735, 697 and 669. δ_H (200 MHz; $CDCl_3$; Me_4Si) 1.53 (3H, t, C(32)H), 2.84 (3H, s, C(21)H), 4.29 (2H, q, C(31)H), 5.53 (2H, s, C(1)H), 7.39 (5H, s, C(12–16)H), 7.47 (1H, d, C(4)H), 7.53 (1H, d, C(5)H); δ_C (50 MHz; $CDCl_3$; Me_4Si) 12.13 (C21), 15.40 (C32), 44.50 (C31), 52.77 (C1), 120.97 (C4), 122.54 (C5), 128.55 (C13,15), 129.33 (C14), 129.54 (C12,16), 132.64 (C11), 143.96 (C2). *m*/*z* (ES$^+$) 201.2, 202.2; *m*/*z* (ES$^-$) 126.9, 261.1, 277.1, 455.3, 456.3; mp onset 86.0 °C, peak 89.1 °C, *J*/g = 73.9.

1-Propyl-2-methyl-3-benzylimidazolium iodide (3). 1-Benzyl-2-methylimidazole (2.46g, 14.37 mmol) and propyl iodide (7 g, 41.2 mmol) were combined to yield 1-propyl-2-methyl-3-benzylimidazolium iodide (3.2g, 65%); ν_{max}(KBr)/cm^{-1} 3165, 3135, 3089, 3064, 2976, 2936, 2872, 1725, 1608, 1581, 1524, 1496, 1469, 1453, 1424, 1384, 1364, 1301, 1263, 1203, 1179, 1154, 1112, 1072, 1044, 1029, 968, 916, 901, 847, 825, 782, 747, 718, 696 and 672; δ_H (200 MHz; $CDCl_3$; Me_4Si) 0.96 (3H, t, C(33)H), 1.40 (2H, m, C(32)H), 2.81 (3H, s, C(21)H), 4.21 (2H, t, C(31)H), 5.56 (2H, s,

C(1)H), 7.38 (5H, s, C(12–16)H), 7.52 (1H, d, C(4)H), 7.53 (1H, d, C(5)H). δ_C (50 MHz; $CDCl_3$; Me_4Si) 11.03 (C33), 12.20 (C21), 23.75 (C32), 50.64 (C31), 52.82 (C1), 121.44 (C4), 121.96 (C5), 128.42 (C13,15), 129.26 (C14), 129.48 (C12,16), 132.56 (C11), 143.87 (C2); *m*/*z* (ES^+) 215.1, 216.1, 277.2, 557.2, 558.2; *m*/*z* (ES^-) 126.9; mp onset 70.8 °C, peak 75.3 °C, *J*/g = 49.8.

1-(*n*-)Butyl-2-methyl-3-benzylimidazolium iodide (4). 1-Benzyl-2-methylimidazole (3.44 g, 20.0 mmol) and *n*-butyl iodide (4.95g, 26.0 mmol) were combined to yield 1-(*n*-)butyl-2-methyl-3-benzylimidazolium iodide (6.4g, 90%); ν_{max}(KBr)/cm^{-1} 3164, 3106, 3077, 2955, 2870, 1725, 1637, 1582, 1525, 1496, 1464, 1385, 1353, 1334, 1299, 1266, 1205, 1185, 1152, 1124, 1075, 1030, 976, 926, 852, 825, 772, 721, 701, 678, 623 and 570; δ_H (200 MHz; $CDCl_3$; Me_4Si) 0.96 (3H, t, C(34)H), 1.40 (2H, m, C(33)H), 1.81 (2H, m, C(32)H), 2.82 (3H, s, C(21)H), 4.19 (2H, t, C(31)H), 5.55 (2H, s, C(1)H), 7.38 (5H, s, C(12–16)H), 7.46 (2H, d, C(4,5)H); δ_C (50 MHz; $CDCl_3$; Me_4Si) 10.57 (C34), 12.93 (C21), 17.23 (C33), 26.25 (C32), 54.42 (C31), 52.89 (C1), 121.08 (C4), 121.82 (C5), 128.62 (C13,15), 129.39 (C14), 129.42 (C12,16), 132.65 (C11), 143.79 (C2); *m*/*z* (ES^+) 229.0, 230.0, 585.2; *m*/*z* (ES^-) 126.6; mp onset 60.9 °C, peak 63.8 °C, *J*/g = 62.0.

1-Pentyl-2-methyl-3-benzylimidazolium iodide (5). 1-Benzyl-2-methylimidazole (2.85g, 16.64 mmol) and pentyl iodide (7.6 g, 38.4 mmol) were combined to yield 1-pentyl-2-methyl-3-benzylimidazolium iodide (2.20g, 36%); ν_{max}(KBr)/cm^{-1} 3168, 3058, 2957, 2926, 2857, 1618, 1584, 1526, 1497, 1455, 1389, 1361, 1330, 1266, 1205, 1178, 1154, 1121, 1088, 1032, 923, 850, 824, 755, 722, 699, 668, 610, 570 and 459. δ_H (200 MHz; $CDCl_3$; Me_4Si) 0.86 (3H, t, C(35)H), 1.27 (4H, m, C(34,33)H), 1.73 (2H, m, C(32)H), 2.89 (3H, s, C(21)H), 4.11 (2H, t, C(31)H), 5.57 (2H, s, C(10)H), 7.40 (5H, m, C(12–16)H), 7.55 (2H, s, C(4,5)H); δ_C (50 MHz; $CDCl_3$; Me_4Si) 10.48 (C35), 12.02 (C21), 18.28 (C34), 21.04 (C33), 32.46 (C32), 52.98 (C10), 57.03 (C31), 121.54 (C4), 122.20 (C5), 128.46 (C13,15), 129.37 (C14), 129.51 (C12,16), 132.17 (C11), 143.70 (C2); *m*/*z* (ES^+) 242.8, 243.8; *m*/*z* (ES^-) 108.0, 126.9, 165.1; mp onset 61.1 °C, peak 65.4 °C, *J*/g = 72.7.

1-(*s*-)Butyl-2-methyl-3-benzylimidazolium iodide (6). 1-Benzyl-2-methylimidazole (3.05g, 17.8 mmol) and *s*-butyl iodide (7.5g, 40.7 mmol) were combined to yield 1-(*s*-)butyl-2-methyl-3-benzylimidazolium iodide (3.47g, 55%); ν_{max}(KBr)/cm^{-1} 3169, 3112, 3089, 2943, 2885, 2870, 1606, 1579, 1522, 1499, 1458, 1389, 1352, 1293, 1272, 1200, 1180, 1154, 1122, 1032, 852, 779, 731, 701, 675, 654 and 616; δ_H (200 MHz; $CDCl_3$; Me_4Si) 0.90 (3H, t, C(34)H), 1.58 (3H, d, C(33)H), 1.89 (2H, p, C(32)H), 2.86 (3H, s, C(21)H), 4.45 (1H, m, C(31)H), 5.59 (2H, s, C(1)H), 7.38 (5H, br-s, C(12–16)H), 7.49 (1H, d, C(4)H), 7.57 (1H, d, C(5)H); δ_C (50 MHz; $CDCl_3$; Me_4Si) 10.52 (C34), 12.36 (C21), 20.74 (C33′), 29.71 (C32), 52.67 (C1), 56.80 (C31), 117.72 (C4), 122.60 (C5), 128.21 (C13,15), 129.10 (C14), 131.34 (C12,16), 134.52 (C11), 143.40 (C2); *m*/*z* (ES^+) 229.0, 230.0; *m*/*z* (ES^-) 126.7; mp onset 134.5 °C, peak 139.4 °C, *J*/g = 80.80.

Instrumental

^1H and ^{13}C NMR spectra were recorded on a Bruker AC-200 MHz spectrometer. Infrared spectra were recorded on a Perkin-Elmer FTIR 1600 instrument. Electrospray mass spectroscopy was carried out on a micromass platform with an electrospray source. Samples were dissolved in either methanol or 1 : 1 methanol/water mixtures. Both positive and negative species were detected. Differential scanning calorimetry was carried out on a Perkin-Elmer DSC-7 calibrated with indium (156.54 °C) and *p*-nitrotoluene (51.64 °C). All melting points for the calibration standards were taken from the onset of the melting.

Structure determinations

Full spheres of 'low'-temperature CCD area-detector diffractometer data were measured (ω-scans, monochromatic Mo Kα radiation, λ = 0.7107$_3$ Å), yielding $N_{t(otal)}$ reflections, these merging to N unique after 'empirical'/multiscan absorption correction (proprietary software) (R_{int} cited). N_o with $I > 2\sigma(I)$ were considered 'observed'. All data were employed in the full matrix least squares refinements on F^2 (reflection weights: $(\sigma^2(F_o^2) + (aP)^2 (+ bP))^{-1}$ ($P = (F_o^2 + 2F_c^2)/3$)), refining anisotropic displacement parameter forms for the non-hydrogen atoms, hydrogen atom treatment following a 'riding' model. (Exception: methyl groups were permitted rotation about their pendant bonds). Neutral atom complex scattering factors were employed within the SHELXL 97 program.[26]

Accessory materials

Detailed crystallographic diagrams and Hirshfeld surface analyses of discrete ion pairs for methyl- (**1**), ethyl- (**2**), propyl- (**3**), (*n*-)butyl- (**4**), pentyl- (**5**) and (*s*-)butyl- (**6**), Fingerprint Plots for methyl- (**1**), propyl- (**3**), (*n*-)butyl- (**4**), and (*s*-)butyl- (**6**), and full crystallographic information files.

Acknowledgements

P.M.D. is grateful to Monash University for a Monash Graduate Scholarship and Monash International Postgraduate Research Scholarship. J.M.P. and D.R.M. are grateful to the Australian Research Council for a QEII Fellowship and Federation Fellowship respectively.

References

1 J. S. Wilkes, J. A. Levisky, R. A. Wilson and C. L. Hussey, *Inorg. Chem.*, 1982, **21**, 1263.
2 D. R. MacFarlane, M. Forsyth, P. Howlett, J. Pringle, J. Sun, G. Annat, W. Neil and E. Izgorodina, *Acc. Chem. Res.*, 2007, **40**, 1165.
3 R. C. Remsing, R. P. Swatloski, R. D. Rogers and G. Moyna, *Chem. Commun.*, 2006, 1271.
4 W. Wang, L. Wu, Y. Huang and B. Li, *Polym. Int.*, 2008, **57**, 872.
5 C. Jin, C. Ye, B. S. Phillips, J. S. Zabinski, X. Liu, W. Liu and J. M. Shreeve, *J. Mater. Chem.*, 2006, **16**, 1529.
6 J. E. Bara, T. K. Carlisle, C. J. Gabriel, D. Camper, A. Finotello, D. L. Gin and R. D. Noble, *Ind. Eng. Chem. Res.*, 2009, **48**(6), 2739.
7 T. Itoh, K. Kude, S. Hayase and M. Kawatsura, *Tetrahedron Lett.*, 2007, **48**, 7774.
8 H. Ohno, *Bull. Chem. Soc. Jpn.*, 2006, **79**, 1665.
9 W. M. Reichert, J. D. Holbrey, R. P. Swatloski, K. E. Gutowski, A. E. Visser, M. Nieuwenhuyzen, K. R. Seddon and R. D. Rogers, *Cryst. Growth Des.*, 2007, **7**, 1106.
10 A. Elaiwi, P. B. Hitchcock, K. R. Seddon, N. Srinivasan, Y.-M. Tan, T. Welton and J. A. Zora, *J. Chem. Soc., Dalton Trans.*, 1995, 3467.

11 W. A. Henderson, V. G. Young, Jr., D. M. Fox, H. C. De Long and P. C. Trulove, *Chem. Commun.*, 2006, 3708.
12 J. G. Huddleston, A. E. Visser, W. M. Reichert, H. D. Willauer, G. A. Broker and R. D. Rogers, *Green Chem.*, 2001, **3**, 156.
13 J. D. Holbrey and K. R. Seddon, *Clean Prod. Process.*, 1999, **1**, 223.
14 I. Lopez-Martin, E. Burello, P. N. Davey, K. R. Seddon and G. Rothenberg, *ChemPhysChem*, 2007, **8**, 690.
15 P. M. Dean, J. Turanjanin, M. Yoshizawa-Fujita, D. R. Macfarlane and J. L. Scott, *Cryst. Growth Des.*, 2009, **9**(2), 1137.
16 H. A. Every, A. G. Bishop, D. R. MacFarlane, G. Oradd and M. Forsyth, *Phys. Chem. Chem. Phys.*, 2004, **6**, 1758.
17 S. Tsuzuki, H. Tokuda and M. Mikami, *Phys. Chem. Chem. Phys.*, 2007, **9**, 4780.
18 H. Weingärtner, *Angew. Chem., Int. Ed.*, 2008, **47**, 654.
19 A. Bondi, *J. Phys. Chem.*, 1964, **68**, 441.
20 M. Deetlefs, C. L. Hussey, T. J. Mohammed, K. R. Seddon, J. van den Berg and J. A. Zora, *Dalton Trans.*, 2006, 2334.
21 P. M. Dean, J. M. Pringle, C. M. Forsyth, J. L. Scott and D. R. MacFarlane, *New J. Chem.*, 2008, **32**, 2121.
22 S. I. Smedley, in *The Interpretation of Ionic Conductivity in Liquids*, Plenium Press, New York, 1980, ch. 3, pp. 82–83.
23 M. A. Spackman and J. J. McKinnon, *CrystEngComm*, 2006, **4**, 378.
24 J. J. McKinnon, D. Jayatilaka and M. A. Spackman, *Chem. Commun.*, 2007, 3814.
25 J. J. McKinnon, A. S. Mitchell and M. A. Spackman, *Chem.–Eur. J.*, 1998, **4**, 2136.
26 G. M. Sheldrick, *Acta Crystallogr., Sect. A: Fundam. Crystallogr.*, 2008, **64**, 112.